

Investigation of local heat fluxes in the contact line area during the growth of a single vapor bubble under microgravity conditions

Anastasia Zorkina^{1,2*}, Fedor Ronshin^{1,2}, Oleg Kabov¹, Alexey Rednikov³, and Lounès Tadrist⁴

¹Kutateladze Institute of Thermophysics, Av. Lavrentyev, 1, Novosibirsk 630090, Russia

²Novosibirsk State University, Pirogova St., 1, Novosibirsk 630090, Russia

³Université libre de Bruxelles, TIPs, CP 165/67, Av. F.D. Roosevelt 50, 1050, Belgium

⁴Aix Marseille Université, CNRS, Laboratoire IUSTI, UMR 7343, 5 rue Enrico Fermi, 13453, France

Abstract. The present work is devoted to the study of heat fluxes from a heating surface into a liquid during single vapor bubble growth. The experiment was conducted as part of the RUBI (Reference mUltiscale Boiling Investigation) boiling project implemented on the International Space Station between 2019 and 2021. Since microgravity increases the spatial and temporal resolution of the problem, this made it possible to study in detail the processes of heat and mass transfer in the area of a three-phase contact line. The paper presents a developed algorithm for determining heat fluxes and the amount of heat transferred from various zones at different experimental parameters: from the contact line area, from the centre under the bubble and from the liquid-vapor interface. In particular, it is shown that it is in the area of the contact line that the maxima of heat fluxes are observed and that evaporation from this area makes a significant contribution to the growth of the bubble (about 50%).

1 Introduction

Boiling is a process used both in everyday life and in many areas of industry. In the chemical industry, in the design of nuclear power plants, in thermal power engineering, medicine, boiling is an integral part in many areas of human life. The physics of boiling depends on many factors: surface roughness, physical and chemical properties of the tested liquid and, despite a long period of study of this process, there is still no complete understanding of it. In recent years, researchers have been focusing on the experimental and numerical study of boiling in its simplest formulation: the growth of a single vapor bubble on the heating surface [1-3]. One of the key parameters that have a significant impact on the boiling process is gravity. Therefore, the most promising and interesting studies are those conducted in microgravity. Microgravity increases the spatial and temporal resolution of the problem, allowing us to study in detail the processes that are masked by buoyancy in terrestrial conditions, for example, microconvection caused by bubble growth or

* Corresponding author: a.zorkina@g.nsu.ru

thermocapillary convection. In addition, conducting experiments in microgravity conditions will create new correlations for future space applications, for example, for refrigeration equipment, as well as research will be useful in the design of two-phase thermal control systems for spacecraft. For a deeper understanding of the physics of boiling, a multiscale experiment RUBI (Reference mUltiscale Boiling Investigation) on the growth of a single bubble under strictly controlled conditions was conducted on the International Space Station [4]. Due to the high heat transfer coefficient, boiling is often used to cool electronic equipment components. As a consequence, a clear understanding of the heat and mass transfer processes from the heater to the single vapor bubble and to the bulk liquid is required.

The purpose of this work is: numerical calculation of heat fluxes from the surface of the heater in a liquid, determination of the amount of heat: transferred from the liquid-vapor interface, from the contact line area, from the centre under the bubble at various experimental parameters.

2 Experimental setup and Methods

The experimental setup is a cell (the sketch is shown in Fig.1.) filled with a dielectric, pre-degassed liquid FC-72 (C_6F_{14}). A 5 mm thick substrate made of barium fluoride crystal, transparent in the IR range, is coated with a layer of chromium nitride (400 nm), which increases the emissivity (the blackness coefficient is close to an absolutely black body) for more accurate temperature measurement with an infrared camera, and chromium (400 nm), which serves as a Joule heater (figure 2). An infrared camera (IR) records the temperature distribution of the heating surface with a frequency of 240 fps located at the bottom of the experimental cell. In the centre of the heater there is a cavity with a diameter of 30 microns and depth of 200 microns, in which, after a certain waiting time t_{wait} upon turning on the heater, a vapor bubble is initialized by the laser system ($t = -t_{wait}$ is the time when the heater is switched on, $t = 0$ s the time when the laser system is switched on, $t_{laser\ pulse} = 20$ ms is the duration of the laser pulse). There is a high-speed black-and-white camera (BW) on the side that registers the shape of bubbles at a frame rate of 500 fps, and a light source on the opposite side. IR and BW cameras start recording 1 second before the laser pulse. The cell is equipped with pressure and temperature sensors inside the liquid and inside the cell body and microthermocouples. A more detailed description of the setup, as well as the methods of preparing and conducting the experiment, is presented in the work of Sielaff et al. [4].

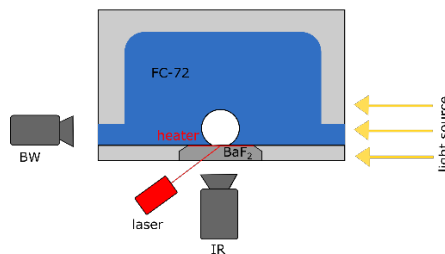


Fig. 1. Experimental setup.

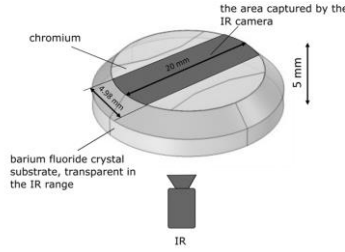


Fig. 2. Heater configuration.

In this paper, heat fluxes from the surface of the heater into the liquid are investigated under various parameters of the experiment: at different pressures (p) of the liquid in the cell ($p = 500; 600; 750$ mbar) and at different preheating (waiting) times of the liquid ($t_{wait} = 2; 5$ s) – the time between turning on the heater and initializing the bubble using a laser pulse. The initial temperature of the liquid is set to T_{set} , close to the saturation temperature (T_{sat}). The subcooling temperature is defined as $T_{sub} = T_{sat} - T_{set}$ and in the considered cases is equal to 1°C . The density of the heat flux from the Joule heater (q_{heat}) averaged over its area is the same for the experiments shown in this work and is equal to 0.5 W/cm². It is treated as a surface heat source (disregarding the thickness of the chromium layers).

Before starting each experiment, the required temperature and pressure values are set in the cell (T_{set}, p) upon thermalization. The maximum temperature inhomogeneity in the cell did not exceed 0.5 °C. Each experiment was repeated 3 times at the specified set of parameters ($p, t_{wait}, T_{sub}, q_{heat}$), which made it possible to largely reduce the appearance of random effects.

To determine the heat fluxes from the surface of the heater into the liquid, the problem of thermal conductivity in a barium fluoride (BaF₂) substrate is solved numerically (equation 1). The solution of the equation is implemented in the Matlab software environment by fractional steps using an implicit finite-difference scheme (equation 2):

$$\frac{\partial T}{\partial t} = a \left(\frac{\partial^2 T}{\partial x^2} + \frac{\partial^2 T}{\partial y^2} + \frac{\partial^2 T}{\partial z^2} \right) \quad (1)$$

$$\frac{T_{ijk}^{m+\frac{1}{3}} - T_{ijk}^m}{\tau} = \frac{a}{h_x^2} \left(T_{i+1jk}^{m+\frac{1}{3}} - 2T_{ijk}^{m+\frac{1}{3}} + T_{i-1jk}^{m+\frac{1}{3}} \right) \quad (2)$$

$$\frac{T_{ijk}^{m+\frac{2}{3}} - T_{ijk}^{m+\frac{1}{3}}}{\tau} = \frac{a}{h_y^2} \left(T_{ij+1k}^{m+\frac{2}{3}} - 2T_{ijk}^{m+\frac{2}{3}} + T_{ij-1k}^{m+\frac{2}{3}} \right)$$

$$\frac{T_{ijk}^{m+1} - T_{ijk}^{m+\frac{2}{3}}}{\tau} = \frac{a}{h_z^2} \left(T_{ijk+1}^{m+1} - 2T_{ijk}^{m+1} + T_{ijk-1}^{m+1} \right),$$

where T is the temperature, a is the thermal diffusivity, τ is the time step, h_x, h_y, h_z are the spatial steps along x, y, z , respectively. The scheme used has a second order in spatial coordinates and a first order in time. The computational domain is a parallelepiped (Fig. 3) with a height of 5 mm, equal to the height of the substrate in the experiment, and transverse dimensions of 4.98 mm x 20 mm, determined by the size of the area captured by the IR camera and the size of the heating surface (Fig. 2). The temperature received from the IR camera is set on the upper wall at each time step, all other walls are assumed to be thermally insulated. The time step τ and spatial steps h_x, h_y , respectively, are determined by the frequency and resolution of the IR camera ($\tau = 0.0042$ s, $h_x, h_y = 0.0415$ mm, and h_z was also chosen to be equal to 0.0415 mm for uniformity).

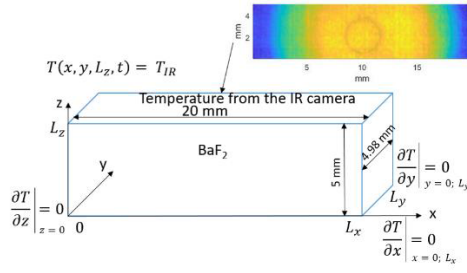


Fig. 3. The computational domain and the boundary conditions.

The temperature distribution recorded by the the IR camera at time $t = 0.2$ s is set as the initial temperature on the upper wall. This point in time was chosen arbitrarily, while allowing not to take into account the influence of the laser pulse (the laser system turns on at time $t = 0$ s, the duration of the laser pulse $t_{laser\ pulse} = 20$ ms), and also not to consider the initial stages of bubble growth, where the determination of heat fluxes is difficult due to the complexity of determining the contact line of the bubble in view of its small volume and insufficient resolution of the IR camera. So, for example, the contact line diameter at time $t = 0.2$ s from the processing of BW images for the case $p = 500$ mbar, $t_{wait} = 2$ s is equal to ~ 0.7 mm which corresponds to 17 pixels. Thus, to determine the initial temperature distribution in the substrate corresponding to the moment $t = 0.2$ s in the experiment, we solve an auxiliary problem of conjugate heat transfer in the substrate and the adjacent liquid layer for the time interval $-t_{wait} < t < 0.2$ s. The equation of thermal conductivity is solved in an axisymmetric formulation to maximize the approximation of the computational domain to the real geometry of the experimental setup (Fig. 2). The computational domain is a cylinder with a radius of 20 mm and a thickness of 10 mm (5 mm is a substrate of barium fluoride BaF_2 , 5 mm is chosen for an adjacent liquid layer of FC-72). For this task: the initial temperature in the entire design area is set equal to T_{set} , the outer walls are thermally insulated, and a constant heat flux density $q_{heat}(r)$ is set on the heating surface (substrate–liquid interface), here the heat flux $q_{heat}(r)$ is recalculated for the axisymmetric case [5,7]. Thus, we obtain the temperature distribution in the substrate at time $t = 0.2$ s. The obtained $T_{initial}$ temperature field is used as an initial condition for determining the heat fluxes from the heater into the liquid during the growth of the vapor bubble at $t > 0.2$ s.

Thus, the temperature distribution inside the substrate is numerically determined at each time step during the entire bubble growth process (bubble growth takes 9 seconds, and then the temperature of the liquid in the experimental cell is decreased, the vapor is condensed and the required p , T_{set} values are set for the next run of the experiment). Considering that all the heat from the heater is shared between the liquid and the substrate, we calculate the heat fluxes that have gone into the substrate and into the liquid:

$$\lambda_{FC-72} \frac{\partial T}{\partial z} - \lambda_{BaF_2} \frac{\partial T}{\partial z} = -q_{heat}(r), \quad (3)$$

where $\lambda_{FC-72}, \lambda_{BaF_2}$ is the thermal conductivity of the liquid and the substrate, respectively.

Using equation (4), we can calculate the total amount of heat required to form a bubble:

$$Q_{total} = \rho_v V(t) \mathcal{L}, \quad (4)$$

where ρ_v is the vapor density, \mathcal{L} is the specific heat of vaporization (both dependent on T_{sat}), and V is the volume of the bubble obtained from the image processing from a black–and–white camera [6].

Using the calculated heat fluxes from the surface of the heater into the liquid, we can obtain the amount of heat: 1) transferred through the area of the three-phase contact line (equation 5); 2) transferred through the centre under the bubble (equation 6); 3) transferred through the liquid-vapor interface (equation 7):

$$Q_{contact\ line} = \int P_{contact\ line} dt, \tag{5}$$

$$Q_{center} = \int P_{center} dt, \tag{6}$$

$$Q_{liquid} = Q_{total} - Q_{contact\ line} - Q_{center}, \tag{7}$$

where $P_{contact\ line}$, P_{center} is the total power allocated from the area of the contact line and from the centre under the bubble (the power allocated in pixels falling into the considered areas is summed up). The the contact line area corresponds to a ring with diameters: $\pm 15\%$ of the diameter of the contact line D_{cl} , where D_{cl} is taken from the processing of IR images (D_{cl} is the diameter of the circle with the lowest average temperature calculated from the ring with diameters $D_{cl}[\text{pixel}] - 0.5$ and $D_{cl}[\text{pixel}] + 0.5$). Accordingly, a circle with a diameter of -15% of the diameter of the contact line was selected for the area of the centre under the bubble. Thus, with this choice of ring diameters ($\pm 15\%$), the characteristic peaks of the heat flux completely fall into the contact line area (Fig. 4).

3 Results

The calculated heat fluxes into the liquid from the heater using the method described in the previous section at various points in time are shown in Fig. 4 (left). Figure 4 on the right shows the values of the angle-averaged heat flow along r at various points in time ($r = 0$ mm corresponds to the centre under the bubble).

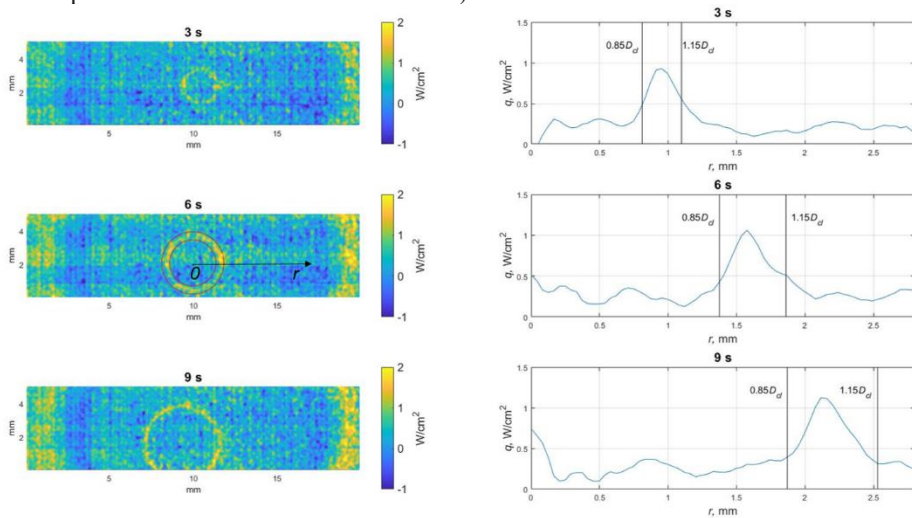


Fig. 4. Heat fluxes (left), heat fluxes along r azimuthally averaged by angle (right). For the case: $p = 500$ mbar, $t_{wait} = 2$ s.

Figure 5 demonstrates: the total amount of heat required to form a bubble of a given volume Q_{total} , the amount of heat transferred across the liquid-vapor interface Q_{liquid} , through the contact line area $Q_{contact\ line}$ and through the centre under the bubble Q_{center} , calculated according to formulas (4)-(7), respectively, for the case of $p = 500$ mbar and $t_{wait} = 2$ s.

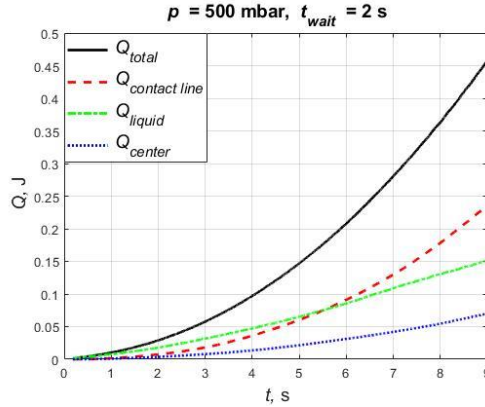


Fig. 5. Contribution to the growth of the bubble from various areas.

As can be seen from Fig. 5, the heat transferred from the contact line area makes a comparable contribution to the heat transferred from the liquid-vapor interface, although it occupies a smaller area compared to the area of the liquid-vapor interface. For example, for the case $p = 500$ mbar, $t_{wait} = 2$ s, the ratio of the area of the liquid-vapor interface to the area of the contact line area is ~ 74 at $t = 0.2$ s and ~ 41 at $t = 9$ s. In the last seconds of bubble growth, the contribution to evaporation from the contact line area reaches 50% ($Q_{contact\ line}/Q_{total} \approx 0.5$). At the initial stages of growth, the contribution from the liquid-vapor interface Q_{liquid} is predominant, since the bubble is still small in volume, it grows completely in the superheated liquid layer (according to estimates made from the numerical solution of the thermal conductivity equation in the substrate and in the adjacent liquid layer, the thickness of the superheated liquid layer is ~ 0.8 mm and ~ 1.3 mm for $t_{wait} = 2$ s and $t_{wait} = 5$ s, respectively, at the time of the laser pulse $t = 0$ s). And also due to the small diameters of the contact lines and the insufficient resolution of the IR camera, it is impossible to accurately calculate the contributions from the contact line and from the centre under the bubble, therefore, at the initial moments of time they may be underestimated. Since initially the temperature of the liquid in the experimental cell is subcooled relative to the saturation temperature by 1°C ($T_{sub} = 1^\circ\text{C}$), vapor condensation can take place in the upper part of the bubble, where the liquid does not have time to warm up yet. Especially in the last seconds of growth, when the height of the bubble by far exceeds the thickness of the boundary layer of the superheated liquid near the heater, which remains small even at the end of the experiment due to the low thermal conductivity of the liquid under study, vapor condensation will occur. As can be seen from Fig. 5, the contribution from the liquid-vapor interface Q_{liquid} is positive, the absolute value of the amount of heat increases during the experiment. This indicates the predominance of evaporation in the lower part of the bubble in the superheated layer over condensation in the upper one, or a possible shift in the saturation temperature (so that the initial temperature of the T_{set} liquid is actually higher than T_{sat} and the liquid is initially overheated), which may partly occur due to the presence of non-condensable gases [7].

Similar results on the study of the contribution of various regions (contact line, liquid-vapor interface and the area under the bubble) to the growth of the bubble were obtained by Schinnerl et al. in [8], where the calculation of heat fluxes was carried out using COMSOL Multiphysics.

Figure 6 illustrates the amount of heat transferred from the contact line area at different p and t_{wait} . As the pressure increases, the amount of heat $Q_{contact\ line}$ decreases:

1) by reducing the specific heat of vaporization \mathcal{L} (from 89.8 kJ/kg at 500 mbar to 86.8 kJ/kg at 750 mbar);

2) by reducing the surface area from which the liquid evaporates (since the vapor density ρ_v increases with increasing pressure, from $\rho_v = 7.02 \text{ kg/m}^3$ at $p = 500 \text{ mbar}$ to $\rho_v = 10.2 \text{ kg/m}^3$ at $p = 750 \text{ mbar}$, which leads to a decrease in the volume of the bubble at the same rate of vaporization; details on how the experimental parameters affect the growth rate of the bubble and, accordingly, its diameter are described in [4]). For example, the ratio of the contact line area at $p = 500 \text{ mbar}$ and $t_{wait} = 2 \text{ s}$ to the contact line area at $p = 750 \text{ mbar}$ and $t_{wait} = 2 \text{ s}$ throughout the bubble growth process is 1.4 (estimated as $(D_{cl}(p = 500 \text{ mbar}))^2 / (D_{cl}(p = 750 \text{ mbar}))^2 \approx 1.4$).

As the preheating time t_{wait} increases, the amount of heat $Q_{contact\ line}$ increases:

1) by increasing the surface area, from which the liquid evaporates (the volume of the bubble increases with an increase in t_{wait} [4]);

2) by increasing wall superheat. For example, the difference of heater temperature between $t_{wait} = 5 \text{ s}$ and $t_{wait} = 2 \text{ s}$ ($p = 500 \text{ mbar}$) in the region of interest at time $t = 0 \text{ s}$ (before the laser pulse) is $\sim 0.8 \text{ }^\circ\text{C}$ (from numerical calculation and processing of IR images).

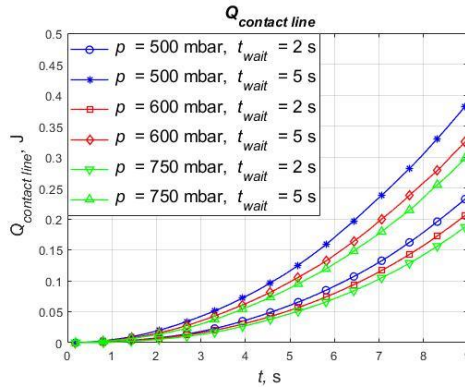


Fig. 6. Dependence of the amount of heat transferred from the contact line area on the experimental parameters (p and t_{wait}).

4 Conclusions

Thus, a numerical algorithm was developed and implemented in the work to determine the heat fluxes from the surface of the heater into the liquid. In particular, special attention was paid to the study of heat fluxes in the contact line area. It is determined that it is in this area that local temperature minima and, accordingly, heat flux maxima are observed, which means that it is in this area that the most intense evaporation occurs. In addition, the amount of heat is calculated: necessary for the formation of a bubble of a given volume Q_{total} , transferred from the contact line area $Q_{contact\ line}$, from the centre under the bubble Q_{centre} and from the liquid-vapor interface Q_{liquid} . From the results obtained, we can conclude that the area of the three-phase contact line makes a significant contribution to the growth of the bubble, although it occupies a smaller area compared to the area of the liquid-vapor interface and the area under the bubble. About 50% of the amount of heat required to form a bubble of this volume is transferred from the contact line area. The influence of the experimental parameters: the pressure of the liquid in the experimental setup p and the preheating time t_{wait} (the time between turning on the heater and initializing the bubble) on $Q_{contact\ line}$ is also studied. With increasing p , the amount of heat decreases by reducing the coefficient of specific heat of vaporization and reducing the surface area from which the liquid evaporates, and with increasing t_{wait} , the amount of heat increases by increasing the surface area from which the liquid evaporates and increasing the gradient temperatures.

Thus, by analyzing the data of the experiment conducted on the ISS, a better understanding of the processes of heat and mass transfer during boiling was achieved. In future work, it is planned to expand the volume of analyzed experimental data, as well as to investigate the influence of other experimental parameters on the amount of heat transferred from the contact line area.

References

1. Y. Nam; J Wu, G Warriar, Y. Sungtaek Ju, Experimental and Numerical Study of Single Bubble Dynamics on a Hydrophobic Surface. *J. Heat Transfer*, **131** (12), 1–7 (2009) <https://doi.org/10.1115/1.3216038/415326>.
2. C. H. M. Baltis, C. W. M. van der Geld, Heat Transfer Mechanisms of a Vapour Bubble Growing at a Wall in Saturated Upward Flow. *J. Fluid Mech.*, **771**, 264–302 (2015) <https://doi.org/10.1017/JFM.2015.174>.
3. A. Surtaev, V Serdyukov, I. Malakhov, A. Safarov, Nucleation and Bubble Evolution in Subcooled Liquid under Pulse Heating. *Int. J. Heat Mass Transf.*, **169**, 120911 (2021) <https://doi.org/10.1016/J.IJHEATMASSTRANSFER.2021.120911>
4. A. Sielaff, D. Mangini, O. Kabov, M. Q. Raza, A. I. Garivalis, M. Zupančič, S. Dehaeck, S. Evgenidis, C. Jacobs, D. Van Hoof, O. Oikonomidou, X. Zabulis, P. Karamaounas, A. Bender, F. Ronshin, M. Schinnerl, J. Sebilliau, C. Colin, P. Di Marco, T. Karapantsios, I. Golobič, A. Rednikov, P. Colinet, P. Stephan, L. Tadrict, The Multiscale Boiling Investigation On-Board the International Space Station: An Overview. *Appl. Therm. Eng.*, **205**, 117932 (2022).
5. M. Schinnerl, A. Sielaff, X. Zabulis, S. Evgenidis, O. O. and S. P. Heat Transfer in Single Bubble Nucleate Boiling within the Multiscale Boiling Project Onboard the International Space Station. In Proceedings of the 17th International Heat Transfer Conference, 14–18 August 2023, Cape Town, South Africa (2023).
6. O. Oikonomidou, S. Evgenidis, C. Argyropoulos, X. Zabulis, P. Karamaounas, M. Q. Raza, J. Sebilliau, F. Ronshin, M. Chinaud, A. I. Garivalis, M. Kostoglou, A. Sielaff, M. Schinnerl, P. Stephan, C. Colin, L. Tadrict, O. Kabov, P. Di Marco, T. Karapantsios, Bubble Growth Analysis during Subcooled Boiling Experiments On-Board the International Space Station: Benchmark Image Analysis. *Adv. Colloid Interface Sci.*, **308**, 102751 (2022) <https://doi.org/10.1016/J.CIS.2022.102751>.
7. F. Ronshin, O. Kabov, A. Rednikov, L. Tadrict, Experimental Investigation of Bubble Growth on a Single Artificial Nucleation Site in Microgravity Conditions: Influence of the Liquid Subcooling and Non-Condensable Residuals. In Proceedings of the 17th International Heat Transfer Conference, 14–18 August 2023, Cape Town, South Africa (2023).
8. M. Schinnerl, A. Sielaff, X. Zabulis, S. Evgenidis, O. Oikonomidou, P. Stephan, & M. Schinnerl, A. Sielaff, X. Zabulis, S. Evgenidis, O. O. and S. P., Heat transfer in single bubble nucleate boiling within the multiscale boiling project onboard the International Space Station. Proceedings of the 17th International Heat Transfer Conference, 14–18 August 2023, Cape Town, South Africa (2023).